IEEJ Journal of Industry Applications
Vol.4 No.4 pp.301–309 DOI: 10.1541/ieejjia.4.301

Paper

Semi-Numerical Method for Calculation of Loss in Foil Windings Exposed to an Air-Gap Field

David Leuenberger[*a)] Non-member, Jürgen Biela[*] Non-member

(Manuscript received July 28, 2014, revised Dec. 22, 2014)

The calculation of eddy current losses in foil windings exposed to a 2-D fringing field is a complex task because of the current displacement along the height of the foil. For model-based optimization of magnetic components, loss calculation with 2-D finite element method simulation is not an option because of the high computational effort. The existing alternative calculation methods with low computational effort, rely on approximations applicable only to a certain geometrical arrangement of the windings and the air gap. Therefore, in this study, a new semi-numerical method was developed to overcome these limitations. The method is based on the mirroring method and is applicable to arbitrary air gaps and winding arrangements. The accuracy of the new method was verified by measurements, and the deviation of the model results from the measured losses was found to be below 15%.

Keywords: air-gap fringing field, eddy current losses, foil winding, magnetic components

1. Introduction

Foil windings feature better thermal properties and a higher copper filling factor than Litz or round wires. On the other hand, foil windings exposed to a 2-D magnetic fringing field are subject to current displacement in two directions, along the thickness *thck* as well as the width *wdth* of the foil, see the example of a foil-inductor in Fig. 1(a) and (b). Calculation methods neglecting the influence of this current displacement suffer from poor modeling accuracy [(1)(2)], as shown for the foil-inductor in Fig. 1(c). To accurately predict the losses in the foil windings, the current displacement must be taken into account, which requires a 2-D field calculation in the winding window. A finite element simulation (FEM) is the most commonly applied approach to perform this 2-D field calculation. Though FEM suffers from long calculation times and difficult parametrization [(1)]. The work in (3), which applied a genetic algorithm to optimize a transformer with foil windings, reported calculation times of 20 hours even for a simplified FEM model considering only one harmonic component. However, for most applications it is inevitable to consider more than one harmonic component for accurate loss prediction. Therefore, FEM is not considered to be an ideal option for automatized model-based optimization. Various alternative methods are proposed in literature to consider the effect of 2-D fringing fields. They can be categorized into two distinct approaches.

The first approach is to derive analytical formulas, which take into account the losses caused by the fringing field and allow for very high calculation speed. The derived formulas rely on an analytical solution of the Maxwell equations in the winding-window. However, to obtain analytically solvable differential-equations, approximations and restrictions to simple geometries are required. The solid-conductor-method proposed in (1), (2) and the method proposed by (5), (6) are the most known methods of this kind. The solid-conductor-method approximates the layers of a foil-winding as one unified solid conductor. The model is shown to be

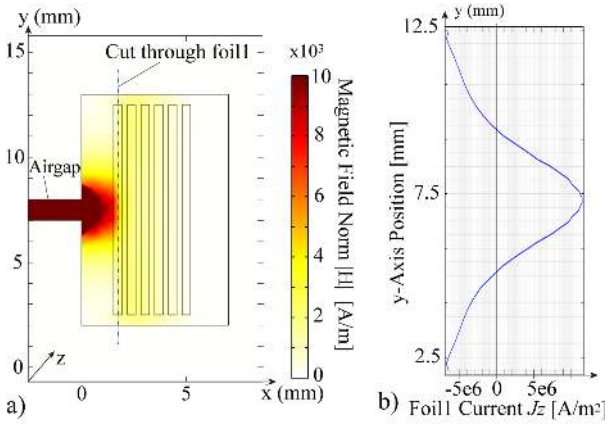

c)

Foil Winding Losses (W/m)	10kHz	30kHz	50kHz
FEM-Simulation:	78mW/m	315mW/m	830mW/m
1D Dowel Method:	65mW/m	242mW/m	560mW/m
DC-Loss ($I^2_{rms}R_{dc}$):		25mW/m	

Fig. 1. FEM Simulation of foil windings in a winding window of a gapped magnetic core (I_{foil} = 5 A/30 kHz): (a) Magnetic field (b) Non-homogeneous current density along foil 1 (see cut-line in Fig. 1(a). The homogeneous current density would be 2.5e6 A/m^2) (c) Losses in the foil winding at 5 Arms sinusoidal winding current at different frequencies in comparison to a simple 1D calculation method [(4)] and the DC-losses

This work has been published at the IPEC-Hiroshima ECCE Asia, May 18th–21th, 2014 under the same title.
a) Correspondence to: David Leuenberger. E-mail: leuenberger@hpe.ee.ethz.ch
* Laboratory for High Power Electronic Systems (HPE) ETH Zurich, Physikstrasse 3, CH-8092, Switzerland

accurate for low frequencies, but at high frequencies the accuracy decreases, because the solid conductor exhibits different eddy currents, than a foil winding would actually have. The method described in (5), (6) approximates the eddy current as line-current-density located at the surface of the foil closest to the gap. This foil is assumed to absorb the whole fringing field. The air-gap is also modelled as line-current-density (by Fourier-decomposition in space). For either of these two methods, the air-gaps must be located at the inner core-leg and the area between the air-gap and the foil-winding must be filled with air or a spacer only (no additional round-conductor winding).

The second approach is often referred to as semi-empirical or semi-numerical. A closed-form formula for the losses is derived from a set of prior FEM simulations. This approach tries to combine the advantages of the FEM-approach - high accuracy and no geometrical restrictions - and the advantages of the analytical-approach - high calculation speed. The squared-field-derivative method, proposed in (7) for round-wires is an example of such a method. The work in (8) derives a modified Dowells-formula [4] for losses in the foil-winding of a high-frequency transformer. The formula contains additional parameters, used to curve-fit the losses from 2-D FEM simulations and enables fast calculation of winding losses. Though, it is restricted to a certain geometry, analyzed prior by FEM simulations.

To be able to effectively perform model-based optimization of magnetic components with foil windings, a method is needed, which features much lower calculation times than a FEM-simulation and on the same time is not subject to restrictions on air-gap and winding arrangement as the existing analytical and semi-numerical approaches. To fulfil this need, in this work a novel, semi-numerical method is developed, which can be applied to arbitrary winding and air-gap geometries. Regarding calculation times, the new method is in between the FEM- and the existing semi-empirical approaches. The developed method can be combined with the mirroring method and is a true 2-D field approximation for foil windings. The method is described in Sect. 2 and its validation is given in Sect. 3.

2. Foil- to Square-Conductor Method

In the following the principle of the calculation method is explained with the example of an inductor with foil windings. Figure 1(a) shows a 2-D finite element simulation of an inductor with a sinusoidal winding current of $I_{z,foil} = 5\,\mathrm{A}@30\,\mathrm{kHz}$. $|H|$ is the amplitude of the 2-D magnetic field introduced by the air-gap. The x-component of the H-field, which is perpendicular to the foils, causes an eddy current flowing in the y-z plane. The existence of the eddy currents results in an inhomogeneous current distribution J_z, which is shown in Fig. 1(b) for the foil closest to the air-gap. For accurate loss modelling, the investigated method must determine the non-homogeneous J_z of every foil of the winding.

The routine to perform this task, consists of two major parts. The first part is the calculation of the non-homogeneous current density $J_{z,foil}$ in a single foil by the following steps shown in Fig. 2:

(1) *Transformation to round-conductors:* The foil is transformed into area-equivalent round-conductors.

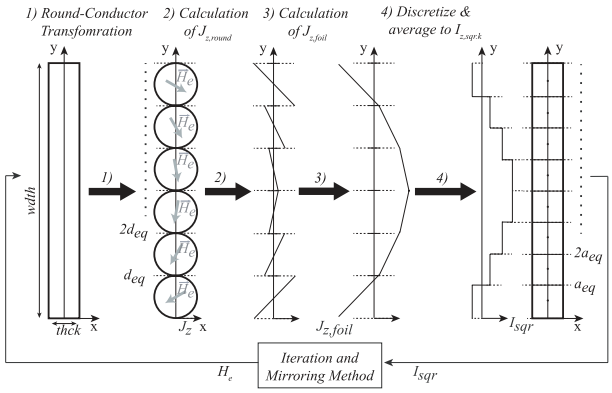

Fig. 2. Overview calculation procedure for non-homogeneous current distribution in a foil, exposed to a 2-D transverse magnetic field: *1)* Round-Conductor Transformation, *2)* Calculation of round-conductor current density, *3)* Calculation of foil current density, *4)* Transformation to square-conductors and calculation of square-conductor currents

(2) *Calculation of current $J_{z,round}$ in round-conductors:* The well known formulas for round conductors are used to calculate the eddy current in each separate round conductor. The external magnetic field H_e is derived using the mirroring method, as will be explained in detail later in this section.

(3) *Calculation of foil current $J_{z,foil}$:* The current density in the foil is derived from the current density of the round conductors, by postulating continuity of $J_{z,foil}$ at the boundary of adjacent round conductors.

(4) *Discretize and average to square-conductors:* The foil is cut into area-equivalent square-conductors. To each square-conductor a current $I_{z,sqr,k}$ is attributed according to $J_{z,foil}$, whereas the current density is approximated to be constant over the cross-section of each square-conductor. Unlike in step 1), a transformation to square-conductors is applied, as they represent the actual foil-winding more accurately. In this way, the current displacement in the foil is taken into account by the square-conductor currents and the mirroring method can be applied to calculate the H-field and the losses in the same way as for round- and Litz-wires [6][9].

The second part of the routine considers the entire foil-winding and involves a numerical iteration to determine $J_{z,foil}$ in each foil of the winding, starting from the uniform distribution. The method is applicable to arbitrary air-gaps and winding arrangements. As the mirroring method is based on a low-frequency approximation ((6) chapter 5.2.1), the model is applicable as long as the foil thickness *thck* fulfills the following condition:

$$thck \leq 1.6 \cdot \delta, \quad (1)$$

where δ is the so called penetration- or skin-depth. The same condition can be alternatively expressed as a frequency limit at a given winding geometry:

$$f_{max} = \frac{2.56 \cdot \rho_c}{\mu \cdot \pi \cdot thck^2}, \quad (2)$$

where ρ_c is the electrical resistivity of the conductor material

and μ the permeability of the material.
The following two sections describe both parts of the routine in detail.

2.1 Non-Homogeneous Current Density in a 2-D Transverse Field The inhomogeneous foil current density $J_{z,foil}$ caused by the 2-D transverse field H_e is calculated with the procedure shown in Fig. 2, which consists of four steps:

2.1.1 Transformation to Round-conductors The foil-winding is transformed into a series of aligned equivalent round-conductors, using the equivalent DC-resistance transformation ((6), chapter 5.4.1 and (10)) and postulating equivalent width $wdth$ of the transformed winding, see Fig. 2, *1)*. The constraints on surface and width can be expressed by $wdth \cdot thck = n_{cond} \cdot \pi \cdot (d_{eq}/2)^2$ and $n_{cond} \cdot d_{eq} = wdth$ from which follows:

$$d_{eq} = \frac{4 * thck}{\pi}. \quad \cdots\cdots (3)$$

2.1.2 Calculation of Current $J_{z,round}$ in Round-conductors With the foil decomposed into aligned round conductors, the eddy current caused by the external magnetic field $\vec{H}_e$ in a round conductor can be calculated using the formula derived in (11) formula (7-45):

$$\bar{J}_z(r,\varphi) = 4\mu_2 H_e j^{\frac{3}{2}} k \frac{J_1(j^{\frac{3}{2}} kr)}{F(j^{\frac{3}{2}} kr_{eq})} sin(\varphi - \varphi_{He}). \quad \cdots\cdots (4)$$

where

$$F(j^{\frac{3}{2}} kr_{eq}) = (\mu_1 + \mu_2) J_0(j^{\frac{3}{2}} kr_{eq}) + (\mu_1 - \mu_2) J_2(j^{\frac{3}{2}} kr_{eq}) \quad \cdots\cdots (5)$$

$$k = \sqrt{(2\pi f)\rho 1 \mu 1} \quad \cdots\cdots (6)$$

and

μ_1 magnetic permeability of the conductor material
ρ_1 conductivity of the conductor material
μ_2 magnetic permeability of material around the conductor
$\vec{H}_e$ sinusoidal transverse magnetic field vector with amplitude H_e and φ_{He}
f frequency of H_e.

Figure 3(a) illustrates a single round-conductor exposed to a transverse H-field. The current density is derived on the y-axis by evaluating the current density at the three points $\left(J_z(r_{eq}, \frac{\pi}{2} - \varphi_{He}), J_z(r_{eq}, -\frac{\pi}{2} - \varphi_{He}), J_z(0,0)\right)$ and linear interpolation, as shown in Fig. 3(b). By assuming, that the aligned round-conductors are isolated from each other, the eddy current J_z along the y-axis is calculated separately for each round-conductor in the transformed foil winding, resulting in the current density shown in Fig. 2, *2)*.

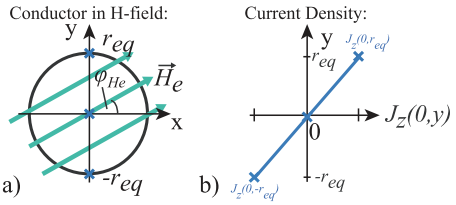

Fig. 3. (a) Round-conductor in a transverse H-field (b) Linearized eddy current density J_z in the round conductor evaluated on the y-axis: $(0,-r_{eq})$, (0,0) and $(0,r_{eq})$

2.1.3 Calculation of Foil Current $J_{z,foil}$ The current density in the foil $\bar{J}_{z,foil}(y)$ $(y = [0, wdth])$ is derived from the eddy currents of the separated round-conductors. Unlike before, the aligned round conductors are now assumed to be electrically connected. Under this condition, the current density must be continuous at the boundary between two conductors. This can be expressed as the following condition, which must hold true for all conductors

$$\bar{J}_{z,k}\left(d_{eq}, \frac{\pi}{2}\right) = \bar{J}_{z,k+1}\left(d_{eq}, -\frac{\pi}{2}\right); k = [1..n_{cond} - 1]. \quad \cdots\cdots (7)$$

As a consequence of Eq. (7), the derivative of the current density $\frac{dJ_{z,foil}(y)}{dy}$ is fully determined by the current density in the round conductors

$$\frac{dJ_{z,foil}(y)}{dy} = \frac{dJ_{z,k}(0,y_k)}{dy}; y_k = mod(y, d_{eq}), k = int\left(1 + \frac{y}{d_{eq}}\right), \quad \cdots\cdots (8)$$

where the function $int()$ rounds down to the next integer. Note that $J_{z,k}$ is given in cartesian coordinates, for the sake of simplicity. A second condition for $J_{z,foil}(y)$ follows from the total current, flowing through the foil winding

$$\int \bar{J}_{z,foil}(y) dA = \bar{I}_{foil}. \quad \cdots\cdots (9)$$

The foil current density $\bar{J}_{z,foil}(y)$ can be calculated considering Eqs. (8) and (9), which is shown schematically in Fig. 2, *3)*.

2.1.4 Discretize and Average to Square-conductors The foil is transformed into n_{sqr} square-conductors with the size $a_{eq} = thck$ as shown in Fig. 2(f). The dimension of the square-conductors is such, that they fulfill the low frequency approximation in Eq. (1). Hence for the mirroring method [12], the square-conductors can be treated in the same manner as windings of round conductors. It is assumed, that the current density in the foil is approximately linear across the crossection of the square conductors. With this assumption the current in each square conductor can be derived from the current distribution $\bar{J}_{z,foil}(y)$ by

$$\bar{I}_{z,sqr,k} = a_{eq}^2 \bar{J}_{z,foil}\left(\frac{a_{eq}}{2} + a_{eq}(k-1)\right). k = [1..n_{sqr}]. \quad \cdots\cdots (10)$$

2.2 Numerical Iteration for entire Foil Winding In Sect. 2.1 a single foil exposed to a sinusoidal transverse field is modelled as n_{sqr} aligned square-conductors with a non-homogeneous current distribution $\bar{I}_{z,sqr,k}, k = [1..n_{sqr}]$. When a magnetic component with an entire foil winding is modelled, the correct determination of the square-conductor currents $\bar{I}_{z,sqr}$ becomes a non-trivial task. This is due to the fact, that a certain calculated $\bar{I}_{z,sqr}$ actually affects its root cause, being the external field $\vec{H}_e$. Therefore a numerical iteration is applied to determine $\bar{I}_{z,sqr}$.
The numerical iteration will again be explained on the example of the inductor with a foil winding, shown in Fig. 1. Each foil is cut into n_{sqr} square conductors. Thus the whole foil winding is represented as $n_{sqr,tot} = n_{sqr} \cdot N_{foil}$ square conductors, where N_{foil} is the turns number of the foil winding.

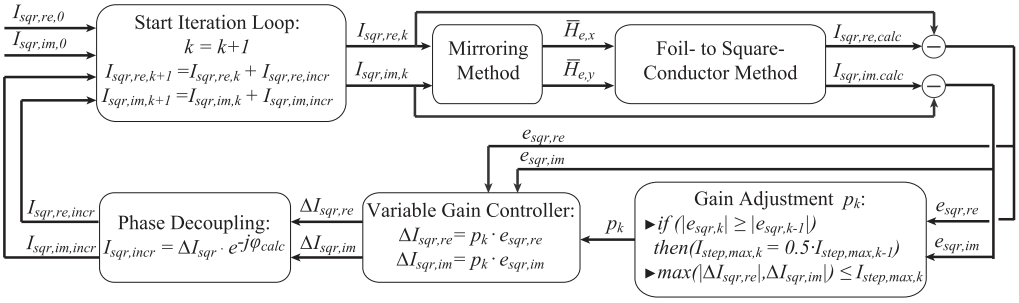

Fig. 4. Overview numerical iteration for calculation of the non-homogeneous current distribution in foil windings

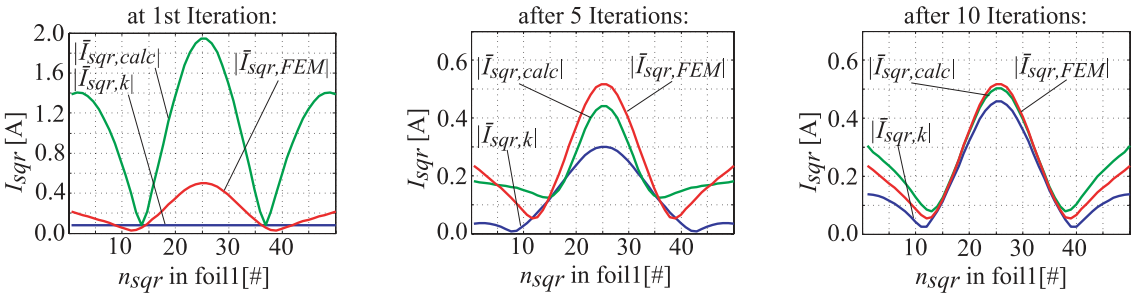

Fig. 5. Numeric iteration for the current in foil 1 of the inductor with foil-winding (shown in Fig. 1): $\bar{I}_{sqr,k}$ and $\bar{I}_{sqr,calc}$ at different iteration-steps in comparison to the current distribution $\bar{I}_{sqr,FEM}$ derived from the 2-D FEM simulation of the inductor

For the winding loss calculation, an arbitrary winding current waveform $i_{foil}(t)$ is decomposed into its complex spectrum by means of the Fourier transform. For each harmonic $\bar{I}_{foil}$ at frequency f_h, the iteration must be performed separately. The complex array $\bar{I}_{sqr}$ of size (1 x $n_{sqr,tot}$) contains the current amplitudes of all square conductors. The starting point of the iteration is the uniform current-distribution:

$$\bar{I}_{sqr,0} = \left[\frac{\bar{I}_{foil}}{n_{sqr}} \dots \frac{\bar{I}_{foil}}{n_{sqr}} \right]. \quad (11)$$

Figure 4 shows the overview of the numeric iteration. At the kth iteration, the latest current-distribution $\bar{I}_{sqr,k}$ is used as input to the mirroring method, to calculate the external H-field at the position of each square conductor $\bar{H}_{e,x}$ and $\bar{H}_{e,y}$. With the foil-to-square-conductor method described in Sect. 2.1, the current distribution $\bar{I}_{sqr,calc}$, that is caused by this external field, is calculated. The expression

$$\bar{I}_{sqr,k} = \bar{I}_{sqr,calc}. \quad (12)$$

is a sufficient condition for the correct current distribution. It describes the situation, where the physical root cause and its effect are in balance. Due to the miscellaneous approximations involved in this method, condition Eq. (12) can not be exactly fulfilled. The goal of the iteration is therefore to minimize the error

$$\bar{e}_{sqr} = | \bar{I}_{sqr,calc} - \bar{I}_{sqr,k} | . \quad (13)$$

This minimization could as well be treated as a purely mathematical problem and state of the art algorithms could be used to determine $\bar{I}_{sqr}$. Though the investigation of such algorithms and the comparison of their performance to the applied iteration-method is out of scope for this work. The applied iterative calculation method for $\bar{I}_{sqr}$ is based on a control-loop analogy. Further it is taken advantage of the fact, that the calculated current distribution $\bar{I}_{sqr,calc}$ exhibits, apart from a proportional scaling factor, approximately the same waveform as the correct current distribution $\bar{I}_{sqr,end}$. This makes it possible to adjust $\bar{I}_{sqr,k}$ by adding an increment $\bar{I}_{sqr,incr}$ derived from $\bar{e}_{sqr}$ at each iteration. Figure 5 illustrates this on the example of the inductor, shown in Fig. 1. The norm of the current distributions in foil 1, $|\bar{I}_{sqr,k}|$ and $|\bar{I}_{sqr,calc}|$ are shown at the very beginning of the iteration and after 5 and 10 iteration steps. The current distribution, $|\bar{I}_{sqr,FEM}|$, derived from a 2-D FEM simulation, is shown as comparison. From the first iteration step on, $|\bar{I}_{sqr,calc}|$ and $|\bar{I}_{sqr,FEM}|$ exhibit similar waveforms and $|\bar{I}_{sqr,k}|$ approaches $|\bar{I}_{sqr,FEM}|$ with advancing iteration.

The detailed function to determine $\bar{I}_{incr}$ from $\bar{e}_{sqr}$ is split into three parts, shown in Fig. 4, which are described in the following:

- *Variable Gain Controller*: To iteratively reduce the error $\bar{e}_{sqr}$, the current distribution is incremented by
$$\bar{\Delta I}_{sqr} = p_k \cdot \bar{e}_{sqr}. \quad (14)$$
- *Gain Adjustment*: The proportional gain p_k is adjusted in each iteration step, in order to limit the maximal current increment per iteration step to $I_{step,max,k}$, hence
$$p_k = \frac{I_{step,max,k}}{max(\bar{e}_{sqr})}. \quad (15)$$
The limit $I_{step,max,k}$ is initialized to the uniform current distribution
$$I_{step,max,0} = \frac{\bar{I}_{foil}}{n_{sqr}}. \quad (16)$$
During iteration $I_{step,max,k}$ is stepwise reduced to ensure, that $\bar{e}_{sqr}$ converges. If the averaged error over the whole winding $\bar{e}_{sqr,avg,k} = \sum \bar{e}_{sqr,k} / n_{sqr,tot}$ did not diminish compared to the error at the last iteration $\bar{e}_{sqr,avg,k-1}$, than $I_{step,max}$ is adjusted:

$$(e_{sqr,avg,k} > e_{sqr,avg,k-1}) \Rightarrow$$
$$I_{step,max,k+1} = \frac{I_{step,max,k}}{2}. \quad \cdots\cdots (17)$$

- *Phase Decoupling*: The feedback-loop introduces a phase-shift, see equation 4 of the foil-to-square-conductor method. To ensure, that the current increment $\bar{\Delta}I_{sqr}$ will actually compensate for the error $\bar{e}_{sqr}$, the phase-shift of the current increment must be compensated by:
$$\bar{I}_{incr} = \bar{\Delta}I_{sqr} \cdot e^{-j\varphi_{calc}} \quad \cdots\cdots (18)$$
where φ_{calc} is the phase-shift of the foil-to-square-conductor method given by:
$$\varphi_{calc} = \angle\bar{I}_{sqr,calc} - \angle\bar{I}_{sqr,k} \quad \cdots\cdots (19)$$

The iteration loop is executed and the current distribution is adjusted by

$$\bar{I}_{sqr,k+1} = \bar{I}_{sqr,k} + \bar{I}_{incr} \quad \cdots\cdots (20)$$

until $\bar{e}_{sqr}$ converges to a negligible small value, having an insignificant influence on the calculated winding losses. Alternatively the winding losses in the whole foil winding can be directly taken as convergence criteria.

$$P_{foil,tot,k} = \sum_{k=1}^{n_{sqr,tot}} P_{sqr,k}, \quad \cdots\cdots (21)$$

$$\Delta_{P,k} = 100\frac{|P_{foil,tot,k} - P_{foil,tot,k-1}|}{|P_{foil,tot,k}|} \quad \cdots\cdots (22)$$

where $P_{sqr,k}$ are the eddy current losses in the kth square-conductor calculated as described in (6). The iteration is stopped, if $\Delta_{P,k}$ stays below a certain threshold over 5 iterations:

$$max(\Delta_{P,k-5}, \ldots, \Delta_{P,k}) \leq 0.1\% \Rightarrow \text{Stop} \quad \cdots\cdots (23)$$

3. Validation of the Proposed Method

The proposed method is validated on the example of a flyback-transformer for a PV-inverter. The whole calculation routine, including the foil-to-square-conductor method, is implemented as software program. The losses in the conductors are calculated according to (13), for Litz-wires, and (6), for square-conductors. The air-gap fringing field is modelled according to (12). The Fourier decomposition of the flyback winding-currents is performed according to (10).

It is important to keep in mind, that the mirroring method restricts the validity of the calculated losses. For accurate calculation of the magnetic field in the winding window Eq. (1) must be fulfilled. This constraint results in a frequency limit f_{max}, that can be calculated for the considered flyback-transformer using Eq. (2). Above this frequency limit the mirroring method overestimates the magnetic field in the winding window and hence the calculated winding losses are subject to a modeling error. Note that a transformer or inductor design, optimized for low winding losses, generally fulfills Eq. (1). Hence Eqs. (1), (2) do not restrict the applicability of the proposed method for a practical design.

The validation is performed twofold, first with a FEM simulation and second with measured losses of a flyback-transformer.

Table 1. Parameters 2-D flyback transformer with foils and Litz-wire

Core	a = 15 mm, c = 7 mm, d = 11 mm
Winding	Cu foil and Litz wires N_1 = 5, $thck_{w1}$ = 0.2 mm, $wdth_{w1}$ = 10 mm N_2 = 50, $d_{s,w2}$ = 0.1 mm, N_s = 7
Air-gap	l_{airgap} = 1mm

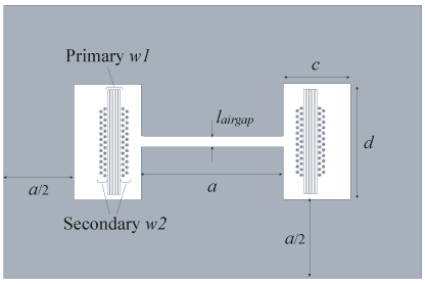

Fig. 6. 2-D Flyback transformer with foils and Litz wires: E-core with air-gap and 'sps' interleaved windings with foils on the primary and Litz wire for the secondary

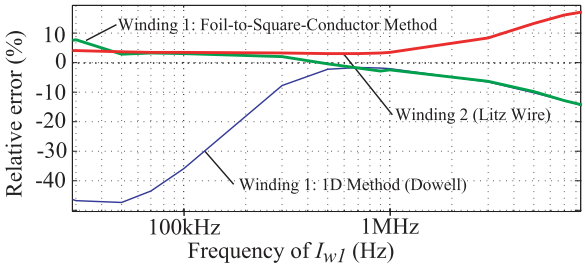

Fig. 7. Flyback-Transformer as specified in Table 1, with sinusoidal excitation of the foil-winding (I_{w1} = 5 A) and open circuit on the secondary: 2D FEM simulation results compared to losses derived from the foil-to-square-conductor method and the 1D calculation method [4]

3.1 Validation with FEM Simulation

The model for foil-winding losses is compared to the conduction losses derived from a 2-D FEM simulation. The specification of the modelled transformer is given in Table 1 and the 2-D winding arrangement is illustrated in Fig. 6. The range of validity for the low frequency approximation of the mirroring method given by Eq. (2), is $f_{max,w1}$ = 270 kHz for the foil winding and $f_{max,w2}$ = 1 MHz for the Litz-wire winding.

A first validation of the loss calculation is performed for the case of a sinusoidal current of 5 A and various frequencies from 10 kHz to 10 MHz flowing through the foil winding. Whereas winding two is an open circuit. The deviation of the new loss model to the 2D FEM simulation is shown in Fig. 7 (in percentage, normed to the FEM simulation values). The losses calculated with the new loss model exhibit good accordance to the 2D FEM simulation. The difference is below 7%, as long as the low frequency approximation is valid, and up to 15% in the whole considered frequency range. Figure 7 further shows the foil losses derived from the simple 1D calculation method [4]. In the frequency range up to 400 kHz, where a typical flyback converter would operate, this method exhibits deviations up to 40% compared to the FEM simulation. For the investigated transformer geometry, the influence of the airgap becomes negligible in the MHz-range with the two methods predicting approximately the same losses.

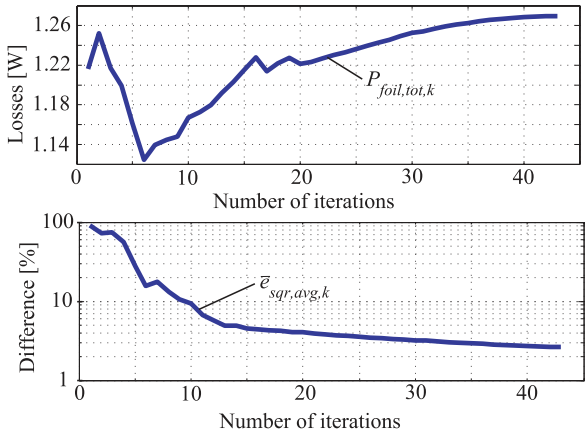

Fig. 8. Loss-calculation for flyback-transformer as specified in Table 1: Iteration convergence of the winding losses in the foil winding $P_{foil,totk,k}$ (see Eq. (21)) and the error in the current distribution $\bar{e}_{sqr,avg,k}$ (averaged over all harmonics and normed to $I_{foil,rms}$, the foil rms-current, see Eq. (13))

Table 2. Comparison foil-to-square-conductor method to 2D FEM simulation for flyback transformer winding losses

Calculation Method	2D FEM Simulation	Foil-to-Square-Cond. Method	
Computer	Laptop, Intel-Core i7-M620@2.67 GHz		
Calculation time	320 s	19 s	113 s
Number of Harmonics	20	20	100
Number of Iterations	-	43	42
Winding Losses P_{w1}	1.32 W	1.28 W	1.33 W
Winding Losses P_{w2}	0.576 W	0.575 W	0.67 W

The second validation is done by considering actual winding current waveforms of a DC-DC flyback converter operating in boundary conduction mode (BCM) at a switching frequency of 100 kHz (8 A peak, 0.75 duty cycle). To limit the FEM calculation time, only harmonics from 100 kHz to 2 MHz are considered. Figure 8 shows the convergence of the error in the non-homogeneous current density $\bar{e}_{sqr,avg,k}$ and the total foil winding losses $P_{foil,tot,k}$ during the iteration (see Sect. 2.2). The error $\bar{e}_{sqr,avg,k}$ converges step-by-step and decreases below 3% after 40 iterations. Simultaneously the calculated losses converge to the final value. After 43 iterations the convergence criteria for the calculated losses Eq. (23) is fulfilled. The final value is 1.28 W, which corresponds to a difference of 3.5% compared to the 2D FEM simulation, see Table 2. To demonstrate the increase in calculation time, a second calculation-run of the foil-to-square-conductor method is performed and also listed in Table 2, taking into account a larger number of harmonics from 100 kHz–10 MHz. The winding losses in the foil increase marginally by 4% due to the higher order harmonic currents.

3.2 Validation with Measured Flyback Transformer

The model for foil-winding losses is verified by measurements on a flyback transformer. The transformer is built with a gapped RM low-profile core and foil windings on the primary and Litz wire on the secondary. First, the measurement setup is described in the following paragraph. The measurement results and the comparison are presented in 3.2.2.

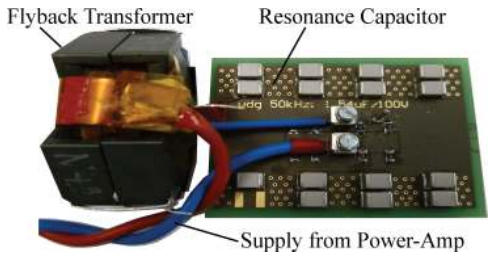

Fig. 9. Experimental setup for winding loss measurement of the flyback transformer.

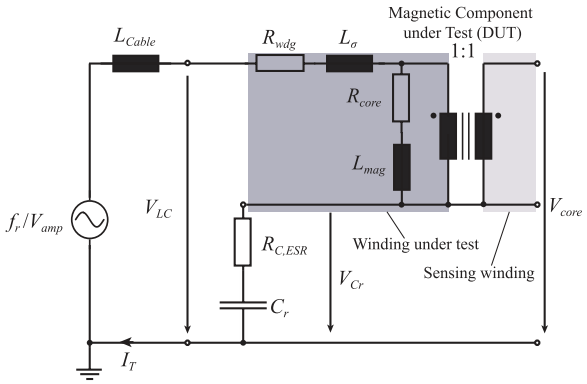

Fig. 10. Overview measurement method for core- and winding-loss measurement of a magnetic component, according to (14)

Table 3. Winding loss measurement setup: used equipment

Waveform Generator	Agilent 33522A
Power Amplifier	AE Techtron 7224
Oscilloscope	LeCroy WaveSurfer 24MXSB
Voltage Probes	LeCroy PP008
Current Probe	LeCroy AP015

3.2.1 Winding Loss Measurement Method and Setup

The measurement-methods proposed in (14) are applied for this verification, which allow to derive the losses in the foil-winding at a sinusoidal winding-current. Figure 9 shows the measurement setup consisting of the flyback transformer and a resonance capacitor. The schematic of the entire measurement setup is shown in Fig. 10 and the applied measurement equipment is listed in Table 3. The primary winding is put in series with a capacitor C_{res} to form a resonant circuit together with the transformers magnetizing inductance. A sinusoidal voltage source, realised with a signal generator and a power amplifier, drives the test current I_{test} through the primary winding. The secondary Litz-winding is left open circuit. The transformer has an additional sensing-winding (0.1 mm^2 Cu round-wire) having the same turns-ratio as the primary winding, which is used for voltage measurements only. Hence no net current is flowing through the sensing-winding. The losses in the sensing winding are negligibly small, due to the low turns-number and the small conductor diameter.

The schematic in Fig. 10 shows the T-equivalent circuit of the transformer, the parasitic cable inductance L_{Cable} and the resonance capacitor series resistance R_{CESR}. The equivalent components of the sensing winding are not relevant, because the winding does not carry any current. L_σ and L_{mag} are the magnetizing- and stray-inductance referred to the primary

winding. The resistors R_{Core} and R_{wdg} model the losses in the core and the primary winding. The aim of the setup is to determine the resistive losses in R_{wdg}. This can be achieved by two distinct measurements.

- *The Resonant Method* as proposed in (15) and described in (14) section 1.2.4, allows to determine the total resistive losses of the resonant-circuit by operating the voltage-source at
$$f_r = \frac{1}{2\pi\sqrt{(L_{mag}+L_\sigma)C_r}}. \cdots\cdots\cdots\cdots\cdots\cdots (24)$$
At this operating point the voltage over L_σ, L_{mag} and C_r cancel out and the voltage measured at the input of the resonant circuit V_{LC} only contains the resistive parts
$$V_{LC} = V_{R,wdg} + V_{R,core} + V_{R,C,ESR}. \cdots\cdots\cdots\cdots (25)$$
Consequently, the losses in the resonance circuit can be split into three parts
$$P_{LC} = P_{R,wdg} + P_{R,core} + P_{R,C,ESR}. \cdots\cdots\cdots (26)$$
The losses caused by the resonance current $P_{LC,fr}$ can be calculated from the measured voltage V_{LC} and current I_T by
$$P_{LC,fr} = \frac{1}{2}\hat{I}_{T,fr}\hat{V}_{LC,fr}\cos(\varphi_{I,T,fr} - \varphi_{V,LC,fr}), \cdots\cdots\cdots\cdots\cdots\cdots (27)$$
where $\hat{I}_{T,fr}$, $\varphi_{I,T,fr}$ and $\hat{V}_{LC,fr}$, $\varphi_{V,LC,fr}$ are the amplitude and phase at the resonance frequency derived from the fourier transform.
- *The Capacitive Cancellation Core Loss Method* proposed in (14) Sect. 2.1.2, can be applied to measure the core losses separately. Unlike the resonant method, where the winding losses are included in the measured losses. The voltage V_{core} is measured between the upper port of the sensing winding to ground, as shown in Fig. 10. Note that the lower port of the sensing winding is connected to the resonance capacitor and hence V_{core} can be expressed as
$$V_{core} = V_{R,core} + V_{L,mag} + V_{R,C,ESR} + V_{C,r}. \cdots\cdots\cdots\cdots\cdots\cdots (28)$$
The frequency of the voltage-source is chosen, such that $V_{L,mag} = -V_{C,r}$, which is the case at
$$f_r = \frac{1}{2\pi\sqrt{L_{mag}C_r}}. \cdots\cdots\cdots\cdots\cdots\cdots\cdots (29)$$
The measured voltage only contains the resistive parts $V_{core} = V_{R,core} + V_{R,C,ESR}$ and the resistive losses caused by the resonance current can be calculated by:
$$P_{core,fr} = \frac{1}{2}\hat{I}_{T,fr}\hat{V}_{core,fr}\cos(\Delta\varphi_{fr}), \cdots\cdots\cdots (30)$$
with
$$\Delta\varphi_{fr} = \varphi_{I,T,fr} - \varphi_{V,core,fr}. \cdots\cdots\cdots\cdots\cdots (31)$$
The losses consists of the following two parts
$$P_{core,fr} = P_{R,core,fr} + P_{R,C,ESR,fr}. \cdots\cdots\cdots\cdots (32)$$

To obtain the magnetic losses $P_{R,wdg,fm}$ at a certain frequency f_m the losses $P_{LC,fm}$ and $P_{core,fm}$ are measured as explained above. For the measured transformer the stray inductance L_σ is much smaller than L_{mag} and hence the same resonant capacitance C_r can be used for both measurements. The magnetic losses can be obtained from the measurements with Eqs. (27) and (32) by:
$$P_{R,wdg,fm} \simeq P_{LC,fm} - P_{core,fm}. \cdots\cdots\cdots\cdots\cdots (33)$$
The losses in $R_{C,ESR}$ cancel out, though $R_{C,ESR}$ should not be much higher than R_{wdg} to obtain a good resolution of the measurement.

The accuracy of the performed loss measurements caused by the deviations in the current Δi, voltage- Δu and phase-angle measurements $\Delta\varphi$ can be deducted from Eqs. (27), (30) using the second-order Taylor-series of the cosine $\left(\cos(x) = 1 - \frac{x^2}{2}\right)$ and neglecting deviation-coefficients of third order:
$$\Delta p_{meas} = \Delta v I + V\Delta i + \Delta v\Delta i - \frac{P}{2}\Delta\varphi^2. \cdots\cdots\cdots\cdots (34)$$
The phase-deviation follows from the time-delay between the voltage- and current-probe by
$$\Delta\varphi = 2\pi \cdot 16ns \cdot f_{meas}, \cdots\cdots\cdots\cdots\cdots\cdots\cdots (35)$$
whereas the time-delay is derived from a reference-measurement using a shunt-resistor. Voltage and current deviation are found to be
$$\Delta v \simeq 80\mu V, \Delta i \simeq 1\,mA. \cdots\cdots\cdots\cdots\cdots\cdots\cdots (36)$$
This is above their theoretical resolution-limit of $63\,\mu$V and $313\,\mu A$, due to the low signal-to-noise ratio at high scale-factors of the oscilloscope. An additional measurement error introduced by the parasitic inter-winding capacitance, described in (14) (2.11), is found to be negligible small, due to the relatively low measuring frequencies. The deviation in the measured winding losses follows from Eq. (33)
$$\Delta p_{wdg} \simeq \Delta p_{LC} + \Delta p_{core}, \cdots\cdots\cdots\cdots\cdots\cdots (37)$$
where Δp_{core} and Δp_{LC} are calculated with Eq. (34).

3.2.2 Loss Measurements and Comparison The flyback transformer loss model is parameterized to model the measured flyback transformer. The frequency limit, up to which the low-frequency 2-D field approximation used for winding loss calculation applies, is determined by Eq. (2) and equals
$$f_{max,low,freq} = 172\,kHz \cdots\cdots\cdots\cdots\cdots\cdots\cdots (38)$$
for the investigated flyback transformer geometry. Above this frequency the modelled winding losses are subject to an increasing modelling error. In Table 4 the measured winding losses are compared to the losses calculated with the model at three different measuring points: 50 kHz, 100 kHz and 200 kHz. Further the accuracy of the measured losses is determined with Eq. (37). The model exhibits a good accordance to the measured losses. The winding losses predicted by the model show a deviation below 15% for the measuring points at 50 kHz and 100 kHz. The measuring frequency of 200 kHz is above $f_{max,low,freq}$ and accordingly the deviation increases to a value of 21%.

Table 4. Flyback transformer winding loss model validation by comparison to measured losses

Frequency: f_{meas}	Loss Measurements: P_{wdg}	Δp_{wdg}	Loss Model: P_{wdg}	Deviation: Δ_{model}
50 kHz	0.0136 W	< ±3.9%	0.0132 W	**−2.6%**
100 kHz	0.0046 W	< ±6.2%	0.0052 W	**14.9%**
200 kHz	0.0022 W	< ±7.5%	0.0026 W	**21.3%**

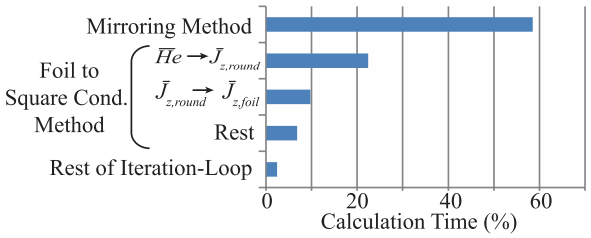

Fig. 11. Flyback transformer model (specification as in Table 1 at DC-DC BCM operation with harmonics from 100 kHz to 2 MHz): calculation complexity analysis

3.3 Calculation Time and Complexity Reducing the calculation speed was a major motivation to develop the foil-to-square-conductor method. The achieved evaluation time for the whole loss-model of a flyback-transformer in DC-DC BCM operation (see 3.1 and Table 1 for specifications), is 19 s and 113 s for a considered number of higher order harmonics of $n_h = 20$ and $n_h = 100$ on a laptop computer equipped with an Intel-Core-i7-620M@2.67 GHz. In comparison, the speed optimized FEM model, using the software FEMM 4.2, exhibits a calculation time of 320s for $n_h = 20$, see Table 2 for details. Figure 11 shows the relative calculation time of the most dominant tasks of the loss-model. The calculation complexity of the foil-to-square-conductor method and the mirroring method scales linearly with n_h and the number of conductors, being $n_{sqr,tot}$ for the foil-to-square and $n_{sqr,tot} + n_{wdg,2}$ for the mirroring method ($n_{wdg,2}$ is the secondary turns number). Note, that all dominant tasks are in the iteration loop (see Fig. 4). Thus the iteration itself is the most time-consuming part of the loss-model, whose calculation time depends linearly on the number of iterations $n_{num,it}$. Evaluations with different parameters showed, that the developed numerical iteration needs an average of $n_{num,it} \simeq 45$ to converge. To further reduce calculation time, an improved iteration-method would be most effective. While $n_{sqr,tot}$ and $n_{wdg,2}$ follow from the specifications, the number of harmonics n_h can be chosen as low as possible, depending on the considered current waveform. A further speed improvement can be achieved in the mirroring method by reducing the number of mirroring below the currently implemented 11x11 mirrored basic winding windows.

4. Conclusion

A new semi-numerical method is developed for loss calculation in foil windings exposed to a 2-D fringing field. Compared to existing calculation methods it features the advantage of much faster calculation speed compared to FEM simulations. For the considered example the calculation time is reduced by a factor of 16. At the same time the new method is not restricted to certain geometric arrangements as the existing analytical and semi-empirical methods. The analysis of the calculation complexity discloses the potential of further speed improvement. The accuracy of the method is validated on the example of a flyback transformer by both FEM simulations and measurements on a test-setup. The method exhibits deviations below 15% in comparison to the measured losses.

References

(1) P. Wallmeier: “Improved analytical modeling of conductive losses in gapped high-frequency inductors”, *IEEE Trans. on Ind. Appli.*, Vol.37, No.4, pp.1045–1054 (2001)

(2) ——: “Automatisierte Optimierung von induktiven Bauelementen für Stromrichteranlagen”, Ph.D. dissertation, Universität Paderborn (2001), Shaker-Verlag, ISBN 3-8265-8777-4.

(3) J. Zwysen, R. Gelagaev, J. Driesen, S. Gooossens, W. Vanvlasselaer, K. Symens, and B. Schuyten: “Multi-objective design of a close-coupled inductor for a three-phase interleaved 140kw dc-dc converter”, in 39th IECON, Vienna (2013)

(4) P. Dowell: “Effects of eddy currents in transformer windings”, Proc. of the Institution of Electrical Engineers, Vol.113, No.8, pp.1387–1394 (1966)

(5) A. Van den Bossche and V. Valchev: “Eddy current losses and inductance of gapped foil inductors”, in IEEE, 28th IECON An. Conference, Vol.2, pp.1190–1195 (2002)

(6) ——, *Inductors and Transformers for Power Electronics*, CRC Press, Taylor and Francis Group (2005)

(7) C. Sullivan: “Computationally efficient winding loss calculation with multiple windings, arbitrary waveforms, and two-dimensional or three-dimensional field geometry”, *IEEE Trans. on Power Electronics*, Vol.16, No.1, pp.142–150 (2001)

(8) F. Robert, P. Mathys, and J.-P. Schauwers: “A closed-form formula for 2D ohmic losses calculation in SMPS transformer foils”, in IEEE 14th APEC, Vol.1, pp.199–205 (1999)

(9) J. Muehlethaler, J.W. Kolar, and A. Ecklebe: “Loss modeling of inductive components employed in power electronic systems”, in Proc. IEEE 8th IPEC (ECCE Asia), pp.945–952 (2011)

(10) J. Zhang, W. Yuan, H. Zeng, and Z. Qian: “Simplified 2-d analytical model for winding loss analysis of flyback transformers”, *Journal of Power Electronics*, Vol.12, No.6, pp.960–973 (2012)

(11) J. Lammeraner and M. Stafl: Eddy Currents, I. B. LTD, Ed. SNTL Publisher of Technical Literature (1966)

(12) J. Muehlethaler, M. Schweizer, B. Robert, J. Kolar, and A. Ecklebe: “Optimal design of LCL harmonic filters for three-phase PFC rectifiers”, *IEEE Trans. on Power Electronics*, Vol.28, No.7, pp.3114–3125 (2013)

(13) F. Tourkhani and P. Viarouge: “Accurate analytical model of winding losses in round litz wire windings”, *IEEE Trans. on Magnetics*, Vol.37, pp.538–543 (2001)

(14) M. Mingkai: “High frequency magnetic core loss study”, Ph.D. dissertation, Virginia Polytechnic Institute and State University (2013)

(15) F. Dong Tan, J. Vollin, and S. Cuk: “A practical approach for magnetic core-loss characterization”, *IEEE Trans. on Power Electronics*, Vol.10, pp.124–130 (1995)

David Leuenberger (Non-member) studied electrical engineering at the Swiss Federal Institute of Technology (ETH) Zurich focusing on Power Electronics and Electrical Drives. After receiving his MSc degree in 2008 he worked as engineer in the area of propulsion control for railway application. Since May 2011 he is pursuing his Ph.D. at the Laboratory for High Power Electronic Systems, focusing on inverters for grid connection of PV systems.

Jürgen Biela (Non-member) received the Diploma (with honors) from Friedrich-Alexander Universitaet Erlangen-Nuernberg, Germany, in 1999 and the Ph.D. degree from ETH Zurich, Switzerland, in 2006. During his studies, he dealt in particular with resonant dc-link inverters at the University of Strathclyde, Glasgow, U.K., and the active control of series-connected IGCTs at the Technical University of Munich, Germany. In 2000, he joined the Research Department, Siemens A&D, Erlangen, where he worked on inverters with very high switching frequencies, SiC components, and EMC. In July 2002, he joined the Power Electronic Systems Laboratory (PES), ETH Zurich, for working toward his Ph.D. degree, focusing on optimized electromagnetically integrated resonant converters. From 2006 to 2007, he was a Postdoctoral Fellow with PES and a Guest Researcher with the Tokyo Institute of Technology, Japan. From 2007 to 2010, he was a Senior Research Associate with PES. Since 2010, he has been an Associate Professor in high-power electronic systems with ETH Zurich. His current research is focused on the design, modeling, and optimization of PFC, dc-dc and multilevel converters with emphasis on passive components, the design of pulsed-power systems, and power electronic systems for future energy distribution.